ORGANIC CHEMISTRY FRONTIERS

RESEARCH ARTICLE

View Article Online
View Journal | View Issue

Cite this: *Org. Chem. Front.*, 2025, **12**, 2607

Dual-state emission of pyrazolyl-pyrrolo[3,4-*b*]pyridin-5-ones *via* excited-state intramolecular proton transfer (ESIPT): multicomponent synthesis and optical characterization†

Julio C. Flores-Reyes,‡[a] Yoarhy A. Amador-Sánchez, ‡[a] Alejandro Valderrama-Celestino,[a] Bertha D. Barrios-Campos,[a] Ricardo A. Peralta, [a] Michael T. Huxley,[b] Ilich A. Ibarra, [c] Alejandro Islas-Jácome, [a] Diego Solis-Ibarra *[c] and Eduardo González-Zamora *[a]

Received 2nd December 2024,
Accepted 17th February 2025

DOI: 10.1039/d4qo02256d

rsc.li/frontiers-organic

The dual-state emission (DSE) phenomenon has become crucial for developing dual-state emission luminogens (DSEgens) that exhibit efficient luminescence in both solution and solid states, addressing the limitations of conventional, phase-restricted fluorophores. Compounds exhibiting excited-state intramolecular proton transfer (ESIPT) mechanisms are especially valuable for enhancing emission stability across these states, offering significant potential in optoelectronics, bioimaging, and sensing applications. In this study, we report the synthesis of six new pyrazolyl-pyrrolo[3,4-*b*]pyridin-5-ones through an Ugi-Zhu-3CR coupled to an aza-Diels–Alder/*N*-acylation/decarboxylation/dehydration cascade sequence. An X-ray ORTEP confirms unequivocally the structure of one of the synthesized compounds. These ones demonstrate intriguing photophysical properties such as large Stokes shifts (>11 900 cm^{-1}) in solution and robust solid-state emission *via* ESIPT mechanism. Complementary DFT and TD-DFT calculations confirm weak but allowed transitions involving both pyrazole and pyrrolo[3,4-*b*]pyridin-5-one moieties, in agreement with experimental observations. This work represents the first application of an isocyanide-based multicomponent reaction for DSEgen synthesis, paving the way for innovative advances in the design of organic luminescent materials.

Introduction

The DSE phenomenon has garnered significant attention within the scientific community due to its potential to enable DSEgens that emit effectively in both solution and solid states.[1] Such materials bridge a critical gap left by traditional fluorophores, which are often restricted to single-phase emission. Achieving efficient DSE requires strategic incorporation of functional groups to sustain emission across varying states. Notably, the integration of triphenylamine (TPA)[2] and tetraphenylethylene (TPE)[3] units has proven effective for their strong emission properties and ability to minimize aggregation-caused quenching (ACQ)[4] by reducing detrimental π–π stacking-type interactions in conjugated aromatic systems.[5] Further, modifications with long-chain C–C organic species create "isolated" solid-state environments, enhancing emission with improved quantum yields. Incorporating aliphatic chains also enhances compound solubility, facilitating solution-processability for device applications and supporting robust DSE behavior.[6] Compounds with ESIPT capabilities are also under active investigation, as this mechanism improves emission stability and intensity in both solution and solid phases. These advancements in DSE design show substantial promise for optoelectronics, bioimaging, and sensing technologies, where stable and versatile emission characteristics are essential.[7]

Alongside, pyrazole-based heteroaromatic compounds have gained significant interest due to their presence in various biologically and industrially important molecules, including

[a]*Departamento de Química, Universidad Autónoma Metropolitana-Iztapalapa, Av. Ferrocarril San Rafael Atlixco 186, Col. Leyes de Reforma 1A Sección, Iztapalapa, 09310 Ciudad de México, Mexico. E-mail: egz@xanum.uam.mx*
[b]*School of Physics, Chemistry and Earth Sciences, Faculty of Sciences, Engineering and Technology, The University of Adelaide, Adelaide, SA, 5005, Australia*
[c]*Laboratorio de Fisicoquímica y Reactividad de Superficies, (LaFReS), Instituto de Investigaciones en Materiales, Universidad Nacional Autónoma de México, Circuito Exterior S/N, CU, Coyoacán, Ciudad de México, Mexico.*
E-mail: diego.solis@unam.mx

†Electronic supplementary information (ESI) available. CCDC 2402623. For ESI and crystallographic data in CIF or other electronic format see DOI: https://doi.org/10.1039/d4qo02256d

‡These authors contributed equally to this work.

natural products,[8] antimicrobial agents,[9] and emissive chromophores.[10] These aromatic systems serve as essential building blocks for the rapid development of optoelectronic devices, such as organic light-emitting diodes (OLEDs).[11] To this end, synthetic strategies that provide high yields and excellent atom economy are highly desirable, enabling the efficient generation of diverse molecular architectures. Among these approaches, multicomponent reactions (MCRs) stand out for their ability to produce key emissive motifs with valuable biological[12] and optical properties[13] while circumventing the limitations of multi-step procedures, such as low yields and labor-intensive purification steps.[14] Moreover, pyrazole-based compounds are particularly appealing for designing luminescent materials due to their neighboring nitrogen atoms, which can act as hydrogen bond acceptors, facilitating highly desirable emissive phenomena like the ESIPT effect.[15] This process begins with the photoexcitation of the material, resulting in the formation of two tautomers (enol and keto forms) with distinct electronic structures. In the ground state these molecules adopt an enol (E) configuration since they are stabilized by an intramolecular hydrogen bond. Upon light absorption, the enol tautomer enters an excited state (E*), during which the electronic charge is redistributed resulting in an increased acidity of the H-donor and an increased basicity of the H-acceptor, causing a proton transfer to occur, generating a new excited keto tautomer (K*). As the system relaxes to its ground state, a recombination mechanism takes place, resulting in light emission (K) distinct than from absorbed in the first step of the ESIPT process. The K form tautomerizes back to the E form by a reverse proton transfer, completing a four-level photochemical cycle (Fig. 1).

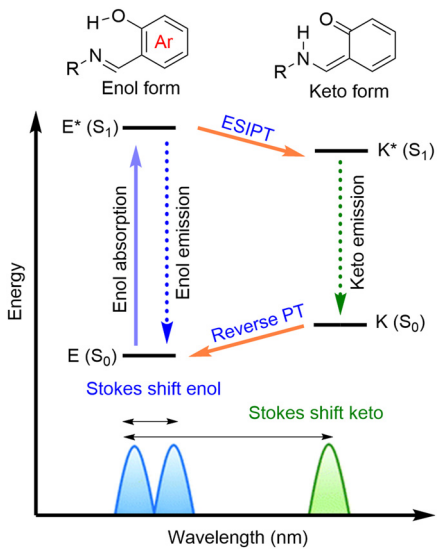

Fig. 1 Representation of the ESIPT mechanism in emissive compounds.

Our research group has previously developed novel methodologies based on the Ugi-Zhu reaction (UZ-3CR), utilizing various amines, aldehydes, and key α-isocyanoacetamides to assemble 5-aminooxazoles.[16] These latter are subsequently subjected to a cascade sequence (intermolecular aza Diels–Alder cycloaddition/*N*-acylation/decarboxylation/dehydration) with maleic anhydride, yielding a series of pyrrolo[3,4-*b*]pyridin-5-ones with promising biological[17] and optical[18] properties (Scheme 1).

As part of our ongoing efforts to synthesize novel and complex polyheterocyclic compounds, we have developed several methodologies that utilize the Ugi-Zhu three-component reaction as a key synthetic tool. This strategy has proven effective for preparing various pyrrolo[3,4-*b*]pyridin-5-one series, either fused, bound, or linked to heterocyclic frameworks of interest for their optical and medicinal properties. In this study, we successfully synthesized a series of pyrazole-derived pyrrolo[3,4-*b*]pyridin-5-one dual-state emitters through an Ugi-Zhu/cascade (aza Diels–Alder/*N*-acylation/decarboxylation/dehydration) sequence with emission in both solution and solid states. To the best of our knowledge, this is the first report in which an isocyanide-based multicomponent reaction has been employed for the creation of DSEgens. Additionally, optical characterization revealed intriguing fluorescence properties, underscoring the potential applications of these compounds in the field of photonics and as bioactive agents.

Results and discussion

Organic synthesis

To access the target pyrazolyl-pyrrolo[3,4-*b*]pyridin-5-one scaffold, we synthesized the corresponding *O*-protected pyra-

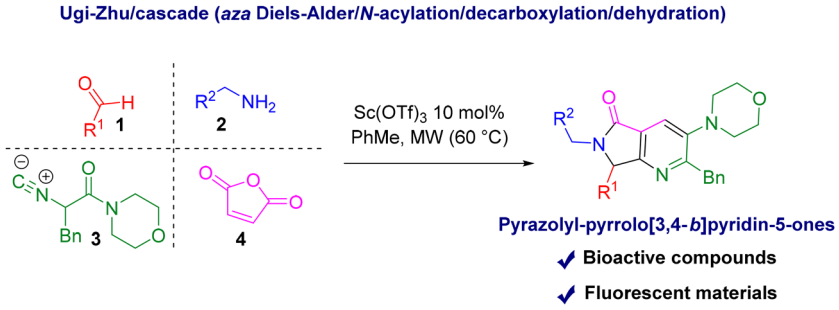

Scheme 1 Ugi-Zhu/aza Diels–Alder sequence for the multicomponent assembly of pyrrolo[3,4-*b*]pyridin-5-ones.

zole-derived aldehyde, which is crucial for the Ugi-Zhu reaction. First, a condensation was performed between phenylhydrazine and 2′-hydroxyacetophenone, followed by the incorporation of the aldehyde moiety using the classic Vilsmeier–Haack protocol, yielding the desired pyrazole **1′** with an isolated yield of 38% in a two-step process. After this, the hydroxy group was protected by introducing the methoxymethyl (MOM) protecting group by reacting the aldehyde with methoxymethyl chloride in the presence of sodium hydride. The MOM-protected aldehyde **1** was obtained in 64% yield (see ESI S1 and S2†).[19] The protection of the hydroxyl group is essential to obtaining the desired compounds, as the reaction does not proceed when using the unprotected aldehyde. We attributed this to an increased resonance stabilization upon the loss of the acidic proton, rendering the aldehyde unreactive toward nucleophilic attack by the amine. With compound **1** in hand, the α-isocyanoacetamide **3** was synthesized following a slightly modified protocol established by Zhu and Bienaymé (see ESI S3†).[16] It is noteworthy that the previously obtained synthetic modules are pivotal for the expedited access to the desired pyrazolyl-pyrrolo[3,4-*b*]pyridin-5-one scaffolds using the Ugi-Zhu/cascade (aza Diels–Alder/*N*-acylation/decarboxylation/dehydration) sequence. As shown in Scheme 2, the multicomponent methodology proceeded efficiently by incorporating the corresponding *O*-protected pyrazole-carbaldehyde **1**, the α-isocyanoacetamide **3**, various aliphatic amines (**2a–f**), and maleic anhydride (**4**) in dry toluene. The reaction was catalyzed by 10 mol% of $Sc(OTf)_3$ under microwave heating (60 °C, 100 W) for 1.5 hours. After purification and isolation, the desired MOM-protected heterocycles **5a–f** were obtained in 22% to 45% yields. At this stage, the MOM deprotection was necessary to obtain the desired ESIPT scaffolds. The MOM deprotection protocol was conducted under mild conditions (0.4 M HCl in THF), yielding the expected **6a–f** products with yields ranging from 42% to 79% (see Scheme 2). Considering factors such as atom economy (up to 84.82%), structural complexity, and the number of steps composing the overall one-pot process, the isolated yields are deemed satisfactory. It is worth noting that all compounds were characterized by ^{1}H, ^{13}C, and ^{19}F NMR, as well as high-resolution mass spectrometry (HRMS). Fortunately, high-quality crystals of compound **6e** were successfully obtained for X-ray diffraction analysis, which unequivocally confirmed its polycyclic structure (see the ESI Table S1† for complete X-ray analysis).

The process begins with a condensation between aldehyde **1** and the primary amines **2a–f**, resulting in the formation of

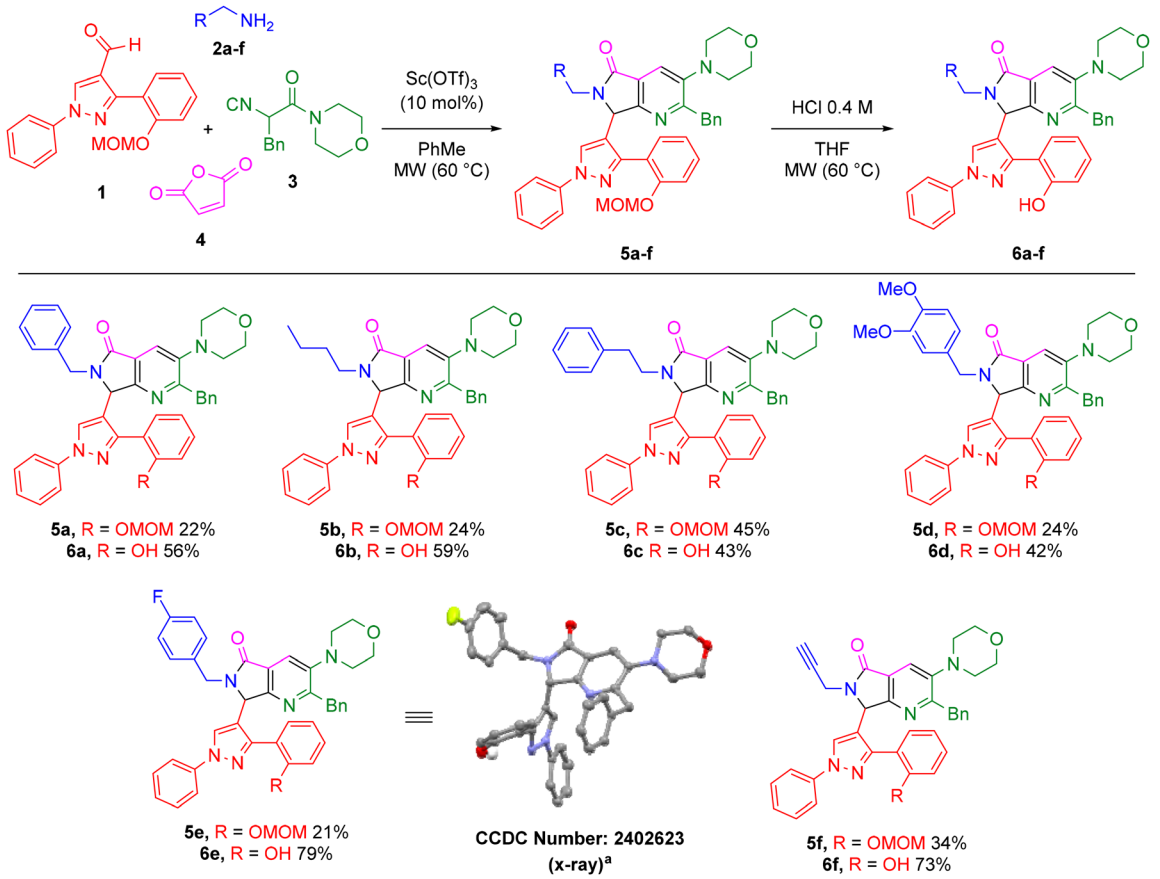

Scheme 2 Pyrazolyl-pyrrolo[3,4-*b*]pyridin-5-ones and their respective deprotections synthetized by an Ugi-Zhu/cascade (aza Diels–Alder/*N*-acylation/decarboxylation/dehydration) sequence. (a) Thermal ellipsoids are drawn at 50% probability, with all hydrogen atoms omitted for clarity, except for the hydrogen atom of the pyrazole moiety (key for the ESIPT photochemical cycle).

imines **7**, which are activated by Sc[III]. This activation promotes α-addition by the isocyanide **3**, leading to the formation of nitrilium ion intermediates **8**. These crucial intermediates are then intramolecularly captured by the amide oxygen through a 5-*endo*-dig cyclization, forming 5-aminooxazoles **10**.[16] The 5-aminooxazoles **10** react with maleic anhydride (**4**) in a cascade sequence of reactions, beginning with an intermolecular aza Diels–Alder cycloaddition producing the oxa-bridged intermediates **11**. These ones undergo an *N*-acylation followed by a decarboxylation, and a final dehydration process, ultimately yielding the target pyrazolyl-pyrrolo[3,4-*b*]pyridin-5-ones **5** (Scheme S5†).

Photophysical properties

To determine the optical properties of compounds **6a–f**, we first measured the absorption spectra of the deprotected pyrazole aldehyde **1** at a concentration of 10^{-5} M. The molar absorptivity coefficients were found to be 1256 M^{-1} cm^{-1} in chloroform ($CHCl_3$), 11 637 M^{-1} cm^{-1} in acetonitrile (MeCN), and 13 342 M^{-1} cm^{-1} in dimethyl sulfoxide (DMSO). Based on these results, we recorded the full absorption and emission spectra in these three solvents. The deprotected compound showed absorption maxima at 254 nm, 275 nm, and 288 nm in $CHCl_3$, MeCN, and DMSO, respectively, indicating a bathochromic shift with increasing solvent polarity. The emission maxima of deprotected **1**, corresponding to its keto form, were observed at 350 nm, 348 nm, and 354 nm, with Stokes shifts of 10 799 cm^{-1}, 7628 cm^{-1}, and 6474 cm^{-1} in $CHCl_3$, MeCN, and DMSO, respectively. Conversely, an additional emission maximum at 308 nm was observed, corresponding to enol emission in both MeCN and DMSO. Fig. 2 presents the normalized absorption and emission spectra in these solvents, while Table 1 summarizes the optical characterization data.

With these data, we proceeded to measure the normalized absorption and emission spectra of compounds **6a–f** in $CHCl_3$ at a concentration of 10^{-5} M (Fig. 3A and B) to compare their optical properties with those of the starting material **1**. A prominent absorption peak at 278 nm, corresponding to the pyrrolo[3,4-*b*]pyridin-5-one core, was observed, along with a secondary, weaker absorption band between 297 and 303 nm, likely due to the pyrazole moiety. The polarity of the solvents had a minor effect on the absorption band positions. In MeCN and DMSO, the bands appeared at nearly identical wavelengths, while $CHCl_3$ exhibited a slight bathochromic shift of 2 to 6 nm relative to MeCN and 4 to 5 nm compared to DMSO (Table 2). The emission spectra of compounds **6a–f** in $CHCl_3$ are shown in Fig. 3B.

Table 1 Summary of photophysical properties of the pyrazole aldehyde **1**

Solvent	Absorption λ_{max} [nm] (ε) [M^{-1} cm^{-1}]	Emission λ_{max} [nm]	Stokes shifts $\Delta\tilde{\nu}$ [cm^{-1}]
$CHCl_3$	254 (12 568)	350	10 799
MeCN	275 (11 637)	348	7628
DMSO	288 (13 342)	354	6313

As shown in Table 2, excitation of compounds **6a–f** at 265 nm revealed that **6b** and **6c** exhibited the highest fluorescence intensity with emission maxima at 422 nm, while compound **6a** displayed the lowest intensity at 419 nm. Notably, compound **6f** demonstrated a bathochromic shift of approximately 11 nm. In general, these compounds exhibited bathochromic shifts with increasing solvent polarity. Compared to their emission in $CHCl_3$, the respective emissions of compounds **6a–f** in MeCN and DMSO occurred at significantly longer wavelengths, suggesting a higher dipole moment in the excited state.[20] When a fluorophore is in the excited state, solvent molecules can relax around the excited dipole by reorienting themselves *via* electrostatic solute-solvent interactions. Higher solvent polarity and an increased excited state dipole moment of the fluorophore will enhance these interactions. This stabilizes and lowers the energy of the excited fluorophore, resulting in a red-shifted emission spectrum. Various excitation wavelengths were tested to acquire these spectra; however, the emission profiles consistently revealed a single emission band, indicating the predominance of one tautomer across the compounds. It is important to note that the Stokes shifts for compounds **6a–f** exceeded

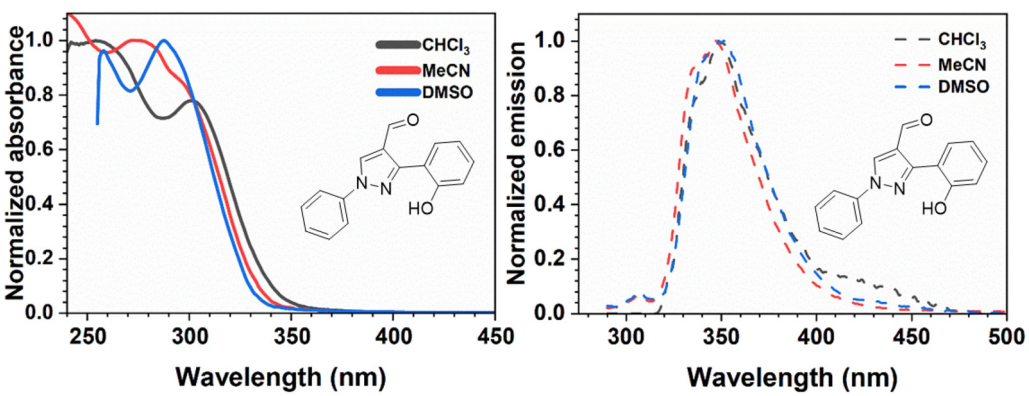

Fig. 2 Absorption (left) and emission (right) spectra of the pyrazole aldehyde **1**, measured at 254 nm, 275 nm, and 288 nm in $CHCl_3$, MeCN, and DMSO, respectively.

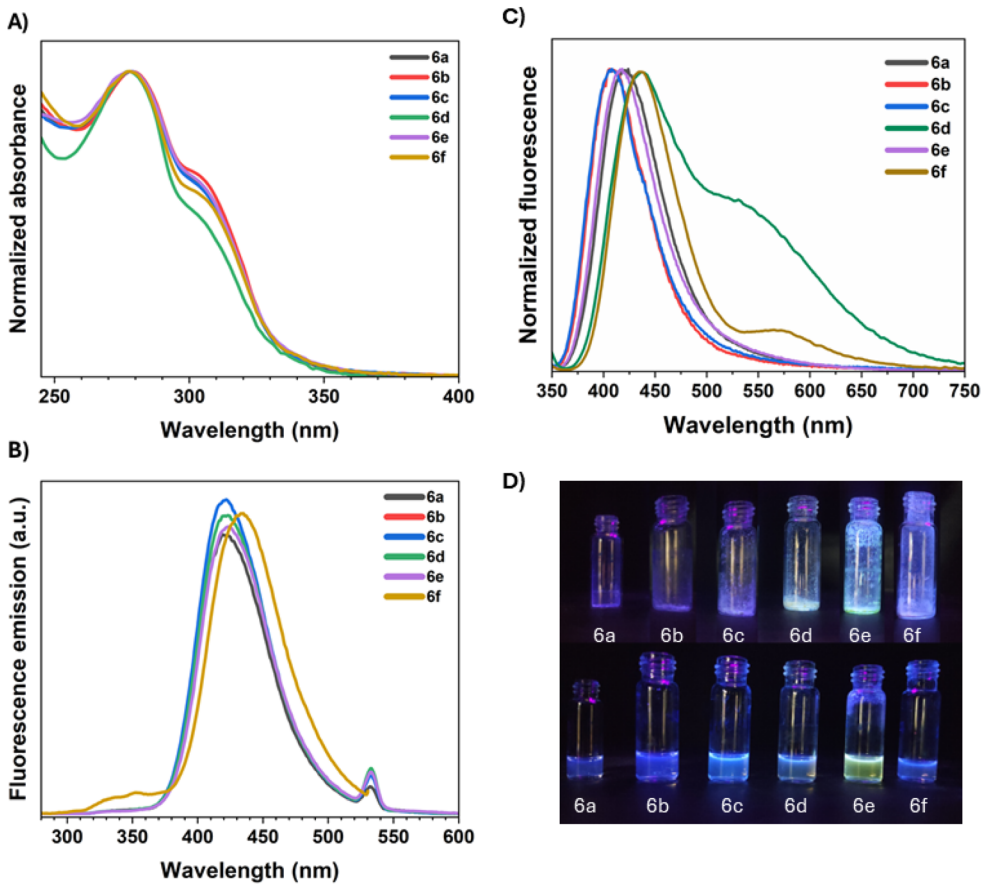

Fig. 3 (A) Absorption, (B) emission espectra of pyrrolo[3,4-*b*]pyridin-5-ones **6a–f** at 10^{-5} M in $CHCl_3$, (C) solid-state emission of compounds **6a–f** λ_{ex} = 343 nm, (D) naked-eye-visible emission of compounds **6a–f** under UV illumination λ_{ex} = 365 nm, observed in the solid-state (top) and in solution (bottom).

11 900 cm^{-1} in all three solvents, particularly in MeCN and DMSO. This observation suggests the potential for an ESIPT, as compounds exhibiting ESIPT typically show large Stokes shifts due to structural differences between the emissive enol and keto forms.[21] However, the presence of a single emission band for both the aldehyde and the products, combined with the large Stokes shifts observed in polar solvents, makes ESIPT unlikely in solution. Proton transfer is expected to be inhibited in such environments, particularly in DMSO. Instead, the observed Stokes shifts are more likely related to the integration of the fluorophore within the pyrrolo[3,4-*b*]pyridin-5-one framework, a phenomenon previously reported in similar systems.[18]

Additionally, the photoluminescence quantum yields (PLQYs) of compounds **6a–f** in chloroform were measured as 1.5%, 2.4%, 2.4%, 1.5%, 1.4%, and 1.6%, respectively. It is noteworthy that all PLQYs were relatively low (<2.5%), indicating a strong preference for non-radiative relaxation pathways (Table 2).[22] In the solid state, however, ESIPT can be modulated by molecular aggregation and restricted vibrational motion, potentially enhancing emission by minimizing non-radiative losses.[23] This phenomenon is exemplified by aggregation-induced emission (AIE) materials, which are typically weakly emissive or non-emissive in solution but become strongly emissive in the solid state due to restricted molecular motion.[5]

For compounds **6b**, **6c**, and **6e**, solid-state emissions were observed at λ_{em} = 407, 407, and 417 nm, respectively, showing blue shifts of 15 nm for **6b** and **6c** and 7 nm for **6e** compared to their emissions in $CHCl_3$ solution. Compound **6a**, however, exhibited nearly identical fluorescence emission maxima in both solution and solid states. Notably, compounds **6d** and **6f** showed a prominent solid-state ESIPT effect, with dual emission bands at 437 and 532 nm for **6d**, and at 435 and 572 nm for **6f**, corresponding to the enol and keto tautomers, respectively, when excited at λ_{ex} = 343 nm and 374 nm. Additionally, solid-state excitation at λ_{ex} = 500 nm enhanced the longer-wavelength maxima, 532 nm for **6d** and 572 nm for **6f** (Fig. 4), supporting the presence of ESIPT and its role in solid-state emission.

In the solid state, compounds **6a–f** exhibited PLQYs of 21.5%, 14.2%, 13.2%, 7.1%, 17.9%, and 11.1%, respectively, demonstrating a substantial enhancement of fluorescence compared to $CHCl_3$ solutions, with increases ranging from 5-fold for **6d** to 14-fold for **6a**. The fluorescence enhancement observed in the solid state among **6a–f** can be attributed to the

Table 2 Optical properties of compounds **6a–f** in both solution and in the solid-state

Compound	Solvent	Absorbance λ_{max} [nm] (ε) [M^{-1} cm^{-1}]	Emission λ_{max} [nm]	Stokes Shifts[a] $\Delta\tilde{\nu}$ [cm^{-1}]	Φ(%)
6a	MeCN	275 (24 525)	444	13 841.1	—
	$CHCl_3$	279 (23 827)	419	11 976.0	1.5
	DMSO	274 (23 712)	447	14 125.0	—
	Solid	—	420	—	21.5
6b	MeCN	275 (25 943)	441	13 687.9	—
	$CHCl_3$	278 (24 153)	422	12 274.5	2.4
	DMSO	274 (24 034)	445	14 024.4	—
	Solid	—	407	—	14.2
6c	MeCN	275 (23 032)	441	13 687.9	—
	$CHCl_3$	278 (22 497)	422	12 274.5	2.4
	DMSO	273 (24 823)	444	14 107.5	—
	Solid	—	407	—	13.2
6d	MeCN	278 (20 892)	442	13 346.8	—
	$CHCl_3$	278 (22 494)	423	12 330.6	1.5
	DMSO	278 (33 064)	448	13 649.8	—
	Solid	—	437, 532	—	7.1
6e	MeCN	272 (22 453)	441	14 089.0	—
	$CHCl_3$	278 (23 072)	424	12 386.3	1.4
	DMSO	278 (23 537)	447	13 599.9	—
	Solid	—	417	—	17.9
6f	MeCN	276 (21 309)	450	14 009.7	—
	$CHCl_3$	278 (18 859)	435	12 982.7	1.6
	DMSO	275 (17 533)	451	14 190.7	—
	Solid	—	435, 572	—	11.1

[a] The Stokes shifts were calculated as $\Delta\tilde{\nu} = 1/\lambda_{max(abs)} - 1/\lambda_{max(em)}$.

restriction of molecular motions and the effective prevention of detrimental π–π stacking, which inhibits non-radiative decay pathways. In the crystal structure of compound **6e**, the pyrazole moiety and the pyrrolo[3,4-*b*]pyridin-5-one core participate in π–π stacking interactions, with centroid-to-centroid distances of approximately 6.897 Å and 4.332 Å, respectively (see the ESI, Fig. S42–S44†). These distances are significantly larger than the typical detrimental π–π stacking distance (~3.35–3.50 Å), supporting the conclusion that the solid-state emission is enhanced due to the absence of strong π–π interactions that would otherwise quench fluorescence.[1,24] Also, similar results have been observed in squaraine-type ESIPT fluorophores reported by Xia and Wang, where solid-state conformations assisted for a ESIPT mechanism suppress π-stacking, leading to low emission in solution but strong fluorescence in the solid state.[25]

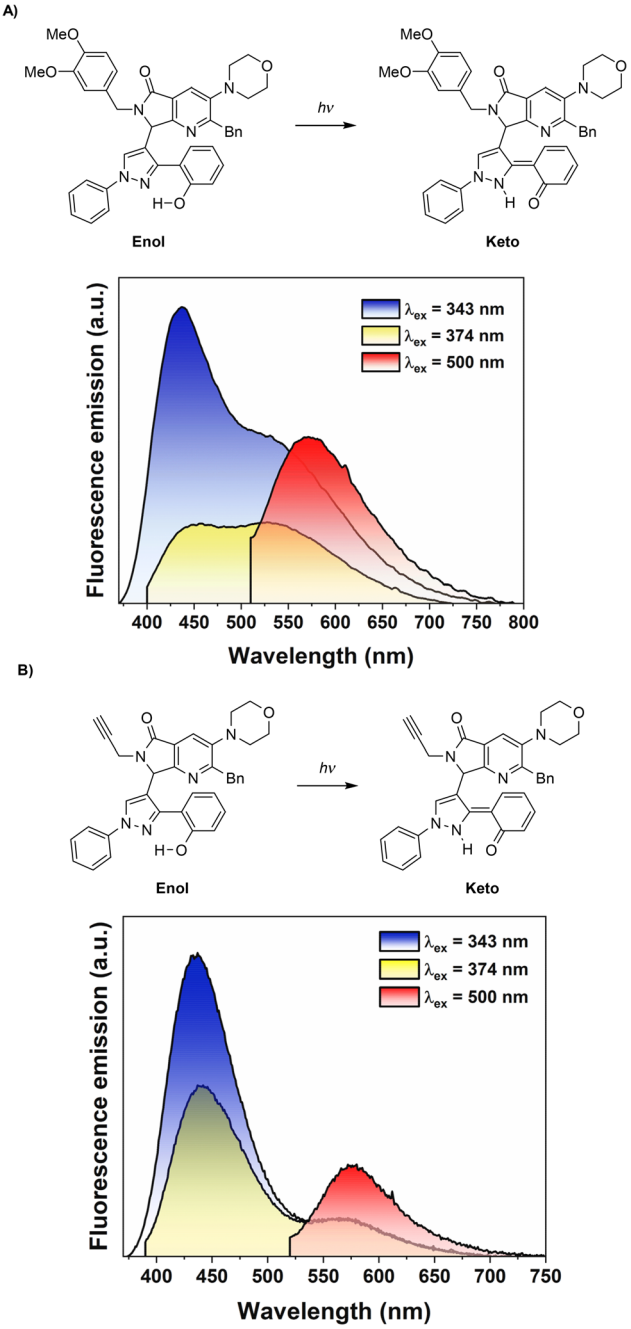

Fig. 4 Solid-state emission spectra at λ_{ex} = 343 nm, 374 nm and 500 nm of compound **6d** (A) and compound **6f** (B).

Electronic structure

The geometries of the ground-state structures of the molecules were optimized through DFT calculations using the Gaussian 09 program,[26] employing the B3LYP functional[27] and the 6-311G(d,p) basis set.[28] The solvation model based on density (SMD) using $CHCl_3$ as solvent was applied to allow comparison with the experimental results. A frequency analysis was performed to ensure that all structures were at an energy minimum and not in a transition state. The theoretical absorption spectra reproduced the experimental results with good accuracy, although all absorption maxima for the pyrrolo[3,4-*b*]pyridin-5-one showed a hypsochromic shift between 3 and 5 nm, while for the pyrazole, there was a bathochromic shift between 6 and 10 nm. The computed oscillator strength values are generally lower compared to those of previous series, indicating that the transitions are weak but allowed. In general, all absorptions are composed of electronic transitions between various orbitals, and notably, in no case is the HOMO → LUMO transition the most significant, unlike other reports of similar systems.[29] The absorption of the pyrazole fragment is

Table 3 Experimental and TD-DFT data on the absorption maxima of compounds **6a–f**. $\lambda_{max,abs}$ (nm)

Compound	Experimental	Calculated	Oscillator strength *f*	Main contributions
6a	279	274	0.192	HOMO−4 → LUMO (21%) HOMO−3 → LUMO (31%) HOMO−2 → LUMO+1 (27%)
	302	310	0.363	HOMO → LUMO+1 (94%)
6b	278	273	0.247	HOMO−3 → LUMO (46%) HOMO−2 → LUMO+1 (34%) HOMO → LUMO3 (10%)
	301	308	0.344	HOMO → LUMO+1 (89%)
6c	278	275	0.260	HOMO−8 → LUMO (16%) HOMO−3 → LUMO (49%) HOMO−2 → LUMO+1 (13%)
	303	309	0.361	HOMO → LUMO+1 (92%)
6d	278	274	0.193	HOMO−8 → LUMO (8%) HOMO−4 → LUMO (49%) HOMO−3 → LUMO+1 (20%)
	303	309	0.323	HOMO−1 → LUMO (10%) HOMO−1 → LUMO+1 (10%) HOMO → LUMO+1 (78%)
6e	278	275	0.186	HOMO−4 → LUMO (24%) HOMO−3 → LUMO (52%) HOMO−2 → LUMO+1 (18%)
	303	310	0.347	HOMO → LUMO+1 (91%)
6f	278	276	0.119	HOMO−2 → LUMO+1 (53%) HOMO → LUMO+2 (38%)
	302	312	0.380	HOMO → LUMO+1 (100%)

predominantly composed of a HOMO → LUMO+1 transition in all cases, while the absorption of the pyrrolo[3,4-*b*]pyridin-5-one is predominantly composed of a HOMO−3 → LUMO transition in compounds **6a**, **6b**, **6c**, and **6e**. For compound **6d**, the predominant transition is HOMO−4 → LUMO, and for compound **6f**, it is HOMO−2 → LUMO+1. These data are summarized in Table 3.

In compounds **6a–c** and **6e**, the HOMO−3 orbital (HOMO−4 for compound **6d**) is distributed over the pyrrolo[3,4-*b*]pyridin-5-one fragment with its substituents, including the benzyl group and the pyrrole substituent, while the LUMO is localized solely on the pyrrolo[3,4-*b*]pyridin-5-one structure with a node at the methine group. For compound **6f**, the most intense absorption consists of two main contributions: one

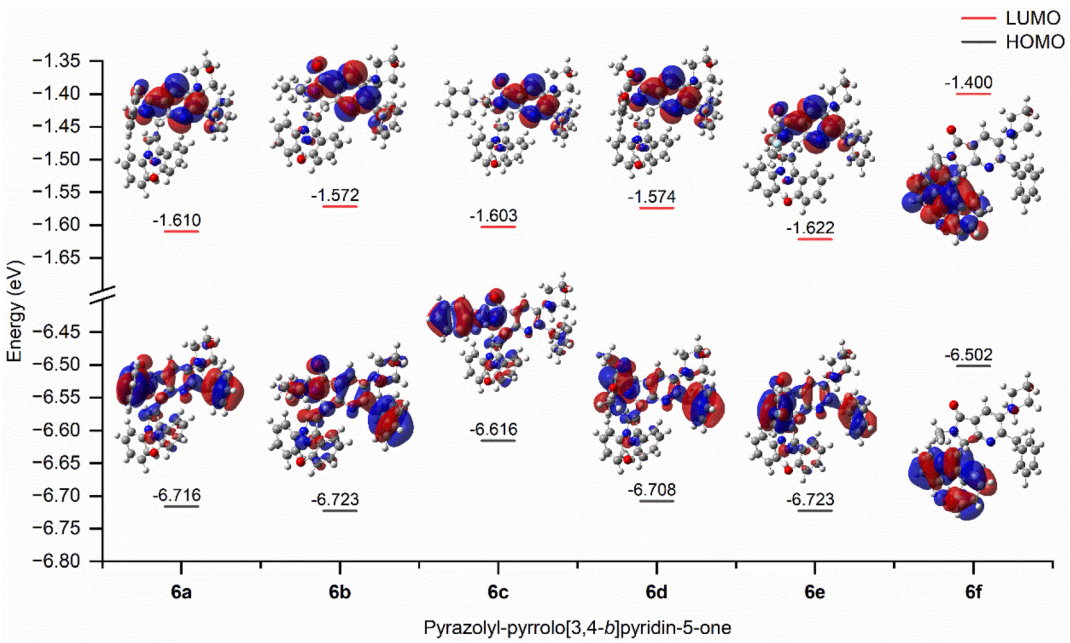

Fig. 5 Representation of the frontier molecular orbitals involved in the strongest absorption band for compounds **6a–f**. For **6a–c** and **6e** HOMO−3 → LUMO is shown. For **6d** HOMO−4 → LUMO is shown. For **6f** HOMO−2 → LUMO+1 is shown.

from the HOMO−2 → LUMO+1 orbital (53%), which is distributed over the pyrazole and its substituents, and the other contribution from the HOMO → LUMO+2 orbital (38%), where the HOMO is localized on the pyrazole and the two rings attached to it, while the LUMO+2 is located on the pyrrolo[3,4-*b*]pyridin-5-one, though in this case, the node is located on the nitrogen of the pyrrole. Fig. 5 shows the distribution of the HOMO and LUMO orbitals involved in the strongest absorption band in the synthesized compounds.

The HOMO distribution is primarily localized within the pyrazole ring, while the LUMO is situated in the pyrrolo[3,4-*b*] pyridin-5-one moiety, indicating that the pyrazole fragment is more electron-rich. Generally, the substituents have little effect on the HOMO energy; however, a greater impact is observed on the LUMO energy. For example, the LUMO of compounds **6b** and **6d** is destabilized by 0.038 eV and 0.036 eV, respectively, relative to compound **6a**. Conversely, the LUMO of compound **6f** is stabilized by 0.014 eV compared to **6a**. These results suggest that no clear relationship can be established between the nature of the substituents and their influence on the LUMO, as no consistent trend is apparent (Fig. S51†).

Conclusions

In closing, in this study six new pyrazolyl-pyrrolo[3,4-*b*]pyridin-5-ones were successfully synthesized in a one-pot fashion coupling a multicomponent Ugi-Zhu reaction to a cascade sequence (aza Diels–Alder/*N*-acylation/decarboxylation/dehydration), achieving isolated yields between 42% and 79%, which are acceptable considering the structural complexity of synthesized polyheterocycles, and that only a couple of molecules of water and one carbon dioxide were released in all synthetic procedure. These compounds exhibited DSE properties. Comprehensive photophysical analysis revealed impressive fluorescence features, including large Stokes shifts in solution and intense solid-state emissions, attributed to restricted intramolecular motions. Notably, the PLQYs were significantly higher in the solid state than in solution, highlighting the beneficial role of molecular conformation in reducing π–π stacking interactions to enhance fluorescence emission. Additionally, some compounds demonstrated a prominent ESIPT, a valuable property for applications requiring stable dual-state emissions. Complementary TD-DFT calculations accurately predicted the absorption maxima, with minor deviations in certain transitions. Electronic structure analysis indicated that the HOMO is predominantly localized on the pyrazole fragment, while the LUMO is centered on the pyrrolo[3,4-*b*]pyridin-5-one scaffold. Substituent modifications had a minimal impact on HOMO energy but significantly influenced LUMO energy. These findings underscore the effectiveness of multicomponent reactions in constructing complex heterocyclic frameworks with tunable optical properties, emphasizing their potential in photonic and bioimaging applications. In summary, the synthetic efficiency, structural diversity, and unique photophysical properties of these pyrazole-derived pyrrolo[3,4-*b*]pyridin-5-ones position them as promising candidates for further investigation in optoelectronic applications, particularly in the development of luminescent materials.

Data availability

The data supporting this article have been included in the ESI.†

Conflicts of interest

There are no conflicts to declare.

Acknowledgements

Authors thank Mónica A. Rincón-Guevara (HRMS), and Atilano Gutierrez-Carrillo (NMR) for spectra. A. I.-J. acknowledges "Proyecto Apoyado por el Fondo Sectorial de Investigación *para* la Educación CONAHCyT-SEP CB-2017-2018 (A1-S-32582)" for financial support. E. G. Z acknowledges DCBI-UAM-I/PEAPDI 2024 for financial support. J. C. F.-R. thanks CONAHCYT for his PhD scholarship (886026). Single-crystal X-ray diffraction data were collected using a Rigaku XtaLAB Synergy-s diffractometer equipped with a HyPix-6000HE detector funded by the Australian Research Council (ARC LE210100163). We are grateful to Prof. A. Paulina Gómora-Figueroa for providing access to the FT-IR instrument.

References

1 J. L. Belmonte-Vázquez, Y. A. Amador-Sánchez, L. A. Rodríguez-Cortés and B. Rodríguez-Molina, Dual-State Emission (DSE) in Organic Fluorophores: Design and Applications, *Chem. Mater.*, 2021, **33**(18), 7160–7184.
2 F. Yu, H. Zhao, Y. Li, G. Xia and H. Wang, D–A-Type fluorophores with efficient dual-state emission for imaging at ultralow concentration, *Mater. Chem. Front.*, 2022, **6**(2), 155–162.
3 Z. Huang, A. Ding, J. Yang, C. Wang and F. Tang, Conjugating Coumarin with Tetraphenylethylene to Achieve Dual–State Emission for Reversible Mechanofluorochromism and Live Cell Imaging, *Chem. – Eur. J.*, 2023, **29**, e202203628.
4 Ein Konzentrationsumschlag der Fluoreszenz, *Z. Phys. Chem.*, 1954, **1**(56), 275–277.
5 J. Mei, N. L. C. Leung, R. T. K. Kwok, J. W. Y. Lam and B. Z. Tang, Aggregation-Induced Emission: Together We Shine, United We Soar!, *Chem. Rev.*, 2015, **115**(21), 11718–11940.
6 L. A. Rodríguez-Cortés, A. Navarro-Huerta and B. Rodríguez-Molina, One molecule to light it all: The era of dual-state emission, *Matter*, 2021, **4**(8), 2622–2624.

7 (*a*) G. Xia, Q. Shao, K. Liang, Y. Wang, L. Jiang and H. Wang, A phenyl-removal strategy for accessing an efficient dual-state emitter in the red/NIR region guided by TDDFT calculations, *J. Mater. Chem. C*, 2020, **8**(39), 13621–13626; (*b*) M. Durko-Maciag, G. Ulrich, D. Jacquemin, J. Mysliwiec and J. Massue, Solid-state emitters presenting a modular excited-state proton transfer (ESIPT) process: recent advances in dual-state emission and lasing applications, *Phys. Chem. Chem. Phys.*, 2023, **25**(22), 15085–15098.

8 V. Kumar, K. Kaur, G. K. Gupta and A. K. Sharma, Pyrazole containing natural products: Synthetic preview and biological significance, *Eur. J. Med. Chem.*, 2013, **69**, 735–753.

9 A. Burke, M. di Filippo, S. Spiccio, A. M. Schito, D. Caviglia, C. Brullo and M. Baumann, Antimicrobial Evaluation of New Pyrazoles, Indazoles and Pyrazolines Prepared in Continuous Flow Mode, *Int. J. Mol. Sci.*, 2023, **24**(6), 5319.

10 A. Tigreros and J. Portilla, Recent progress in chemosensors based on pyrazole derivatives, *RSC Adv.*, 2020, **10**(33), 19693–19712.

11 (*a*) I. v. Taydakov, A. A. Akkuzina, R. I. Avetisov, A. v. Khomyakov, R. R. Saifutyarov and I. Ch, Avetissov, Effective electroluminescent materials for OLED applications based on lanthanide 1.3-diketonates bearing pyrazole moiety, *J. Lumin.*, 2016, **177**, 31–39; (*b*) M. Jin, Y. Chen, W. Song, H. Lian, H. Guo, Q. Dong, J. Huang and J. Su, Synthesis, characterization, and electroluminescent properties of indazole, pyrazole, and triazole/triphenylamine-based compounds, *Dyes Pigm.*, 2020, **173**, 106912.

12 A. Dömling, W. Wang and K. Wang, Chemistry and Biology of Multicomponent Reactions, *Chem. Rev.*, 2012, **112**(6), 3083–3135.

13 L. Levi and T. J. J. Müller, Multicomponent syntheses of functional chromophores, *Chem. Soc. Rev.*, 2016, **45**(10), 2825–2846.

14 (*a*) I. A. Ibarra, A. Islas-Jácome and E. González-Zamora, Synthesis of polyheterocycles *via* multicomponent reactions, *Org. Biomol. Chem.*, 2018, **16**(9), 1402–1418; (*b*) J. C. Flores-Reyes, V. d. C. Cotlame-Salinas, I. A. Ibarra, E. González-Zamora and A. Islas-Jácome, Pseudo-multicomponent reactions, *RSC Adv.*, 2023, **13**(24), 16091–16125; (*c*) J. C. Flores-Reyes, A. Islas-Jácome and E. González-Zamora, The Ugi three-component reaction and its variants, *Org. Chem. Front.*, 2021, **8**(19), 5460–5515.

15 D. Udhayakumari, P. Jerome, N. Vijay and T. H. Oh, ESIPT: An approach and future perspective for the detection of biologically important analytes, *J. Lumin.*, 2024, **267**, 120350.

16 X. Sun, P. Janvier, G. Zhao, H. Bienaymé and J. Zhu, A Novel Multicomponent Synthesis of Polysubstituted 5-Aminooxazole and Its New Scaffold-Generating Reaction to Pyrrolo[3,4-*b*]pyridine, *Org. Lett.*, 2001, **3**(6), 877–880.

17 (*a*) I. Morales-Salazar, F. P. Montes-Enríquez, C. E. Garduño-Albino, M. A. García-Sánchez, I. A. Ibarra, Y. Rojas-Aguirre, M. E. García-Hernández, R. E. Sarmiento-Silva, S. L. Alcaraz-Estrada, E. Díaz-Cervantes, E. González-Zamora and A. Islas-Jácome, Synthesis of bis-furyl-pyrrolo[3,4-*b*]pyridin-5-ones *via* Ugi–Zhu reaction and *in vitro* activity assays against human SARS-CoV-2 and *in silico* studies on its main proteins, *RSC Med. Chem.*, 2023, **14**(1), 154–165; (*b*) I. Morales-Salazar, C. E. Garduño-Albino, F. P. Montes-Enríquez, D. A. Nava-Tapia, N. Navarro-Tito, L. D. Herrera-Zúñiga, E. González-Zamora and A. Islas-Jácome, Synthesis of Pyrrolo[3,4-*b*]pyridin-5-ones via Ugi–Zhu Reaction and In Vitro–In Silico Studies against Breast Carcinoma, *Pharmaceuticals*, 2023, **16**(11), 1562; (*c*) I. Morales-Salazar, C. E. Garduño-Albino, F. P. Montes-Enríquez, A. Gutiérrez-Carrillo, Y. Rojas-Aguirre, N. V. Estrada-Toledo, J. Sandoval-Basilio, S. L. Alcaraz-Estrada, E. Díaz-Cervantes, E. González-Zamora and A. Islas-Jácome, In Vitro and In Silico Studies of Bis-furyl-pyrrolo[3,4-*b*]pyridin-5-ones on Dengue Virus, *J. Mex. Chem. Soc.*, 2024, **68**(1), 170–183.

18 (*a*) J. C. Flores-Reyes, S. M. Rojas-Montoya, L. Blancarte-Carrazco, E. Xochitiotzi-Flores, C. A. Guarin, N. Farfán, A. Galano, A. Islas-Jácome and E. González-Zamora, Multicomponent synthesis and photophysical properties of meso-thienyl BODIPY-pyrrolo[3,4-*b*]pyridin-5-ones. An experimental and theoretical study, *J. Lumin.*, 2024, **273**, 120698; (*b*) J. C. Flores-Reyes, A. Galano, S. M. Rojas-Montoya, L. Blancarte-Carrazco, E. Xochitiotzi-Flores, H. García-Ortega, N. Farfán, A. Islas-Jácome and E. González-Zamora, Synthesis of BODIPY-pyrrolo[3,4-*b*]pyridin-5-ones via Ugi-Zhu/cascade reactions and studies of fluorescence response toward viscosity, *Front. Chem.*, 2024, **12**, 1488933.

19 I. Ali, A. Haque, K. Saleem and M. F. Hsieh, Curcumin-I Knoevenagel's condensates and their Schiff's bases as anticancer agents: Synthesis, pharmacological and simulation studies, *Bioorg. Med. Chem.*, 2013, **21**(13), 3808–3820.

20 A. Kawski, On the Estimation of Excited-State Dipole Moments from Solvatochromic Shifts of Absorption and Fluorescence Spectra, *Z. Naturforsch., A: Phys. Sci.*, 2002, **57**(5), 255–262.

21 A. C. Sedgwick, L. Wu, H.-H. Han, S. D. Bull, X.-P. He, T. D. James, J. L. Sessler, B. Z. Tang, H. Tian and J. Yoon, Excited-state intramolecular proton-transfer (ESIPT) based fluorescence sensors and imaging agents, *Chem. Soc. Rev.*, 2018, **47**(23), 8842–8880.

22 K.-L. Wong, J.-C. G. Bünzli and P. A. Tanner, Quantum yield and brightness, *J. Lumin.*, 2020, **224**, 117256.

23 V. S. Padalkar and S. Seki, Excited-state intramolecular proton-transfer (ESIPT)-inspired solid state emitters, *Chem. Soc. Rev.*, 2016, **45**(1), 169–202.

24 (*a*) J. Shi, L. E. Aguilar Suarez, S. J. Yoon, S. Varghese, C. Serpa, S. Y. Park, L. Lüer, D. Roca-Sanjuán, B. Milián-Medina and J. Gierschner, Solid State Luminescence Enhancement in π-Conjugated Materials: Unraveling the Mechanism beyond the Framework of AIE/AIEE, *J. Phys. Chem. C*, 2017, **121**(41), 23166–23183; (*b*) K. Shirai, M. Matsuoka and K. Fukunishi, Fluorescence quenching by intermolecular π–π interactions of 2,5-bis(*N,N*-dialkyla-

mino)-3,6-dicyanopyrazines, *Dyes Pigm.*, 1999, **42**(1), 95–101.

25 Q. Shao, K. Liang, H. Ling, Y. Wang, Z. Yan, G. Xia and H. Wang, Tetraphenylethylene-incorporated squaraine dyes: structural and theoretical insights into the diverse emission behaviors in solution and solid state, *J. Mater. Chem. C*, 2020, **8**(13), 4549–4556.

26 M. J. Frisch, *et al.*, *Gaussian 09, Revision B.01*, Gaussian, Inc., Wallingford CT, 2010.

27 (*a*) A. D. Becke, Density–functional thermochemistry. III. The role of exact exchange, *J. Chem. Phys.*, 1993, **98**, 5648–5652; (*b*) C. Lee, W. Yang and R. Parr, Development of the Colle-Salvetti correlation-energy formula into a functional of the electron density, *Phys. Rev. B: Condens. Matter Mater. Phys.*, 1988, **37**, 785.

28 R. Krishnan, J. S. Binkley, R. Seeger and J. People, Self–consistent molecular orbital methods. XX. A basis set for correlated wave functions, *J. Chem. Phys.*, 1980, **72**, 650–654.

29 (*a*) H. Zhuang, W. Shi, G. Zhao and Y. Li, Regulating and controlling the stepwise ESDPT channel of $BP(OH)_2DCEt_2$ using the strategy of solvent polarity and external electric field, *Phys. Chem. Chem. Phys.*, 2024, **26**, 12016–12026; (*b*) X. Xin, W. Shi, G. Zhao and Y. Li, Effectively regulation of the ESIPT process via ring-annelation modification for schiff base derivatives: A theoretical study, *Dyes Pigm.*, 2024, **224**, 112020.

